BMC Neurology

RESEARCH Open Access

A novel neutrophil extracellular traps related diagnostic signature for intracranial aneurysm

Xiangmao Zhang[1†], Hanhan Feng[1†], Zongxiang Li[1], Chunying He[1], Junxiang Cui[2], Jinyang Li[2] and Yu Han[1*]

Abstract

Neutrophil extracellular traps (NETs) released by neutrophils can exacerbate inflammation, leading to rupture of intracranial aneurysms (IA). This study aims to explore potential NETs-related genes in IA. RNA sequencing data for IA were downloaded from the Gene Expression Omnibus database. NETs-related genes were screened using weighted gene co-expression network analysis (WGCNA) and differentially expressed gene (DEG) analyses. Gene Ontology (GO) and Kyoto Encyclopedia of Genes and Genomes (KEGG) enrichment analyses were performed. LASSO Cox regression analysis identified optimal genes for model construction. Immune cell infiltration in IA was studied using CIBERSORT. Five NETs-related hub genes were identified in IA, involved in pathways like neutrophil chemotaxis, Toll-like receptor signaling, and regulation of inflammatory response. A risk score model was developed based on TLR7, TLR2, IL1B, ENTPD4, and FPR1. Immune cell infiltration analysis showed significant variations between low-risk-IA and high-risk-IA groups. Monocytes and neutrophils infiltration proportions were significantly positively correlated with the risk score. The ROC analysis showed AUC values exceeding 0.85 for both training and validation sets, confirming the model's excellent performance. A novel NETs-related diagnostic signature for IA was created, offering new insights into the pathogenesis and diagnosis of IA.

Keywords Intracranial aneurysm, NETs, Hub genes, Risk score, Immune cell infiltration

Introduction

Intracranial aneurysm (IA) is an angiogenic disease triggered by expansion of the arterial wall due to elastic membrane damage and destruction of the media within the arterial wall [1]. This condition affects approximately 2–5% of the general population [2]. IA has the potential to cause non-traumatic subarachnoid hemorrhage (SAH), a condition that can lead to severe central nervous system and other organ damage, potentially resulting in life-threatening outcomes [3, 4]. Fortunately, with advancements in medical imaging technology and nerve intervention, unruptured intracranial aneurysms (UIA) are being detected more frequently, significantly enhancing patient survival rates [5]. Despite these improvements, patients with IA still encounter uncommon but significant challenges following endovascular treatment, including bleeding and recurrence [6, 7]. Given that most IA cases are asymptomatic until rupture occurs, early detection of IA is crucial for monitoring its progression and implementing preventive measures [8]. This requires a deeper understanding of the underlying molecular mechanisms involved.

The pathological mechanisms underlying the formation and progression of IA remains incompletely understood.

†Xiangmao Zhang and Hanhan Feng contributed equally to this work as co-first authors.

*Correspondence:
Yu Han
hanyuscience@126.com
[1]Department of Neurosurgery, Zibo Central Hospital, No.54 West Gongqingtuan Road, Zhangdian District, Zibo 255036, Shandong Province, P.R. China
[2]School of Clinical Medicine, Shandong Second Medical University, Weicheng District, Weifang 261053, Shandong Province, P.R. China

Current knowledge has indicated that the recruitment and infiltration of immune cells play a vital part in IA [9, 10]. For instance, the accumulation of immune cells, such as macrophages [11], and immune-related molecules, including interleukin [12] and chemokines [13], could lead to dysregulation of the local immune microenvironment. Interventions targeting the immune inflammatory response and immune microenvironment have been shown to significantly reduce secondary brain damage, thereby improving outcomes for patients with SAH [14]. Despite these findings, the exact role of immune cells and immune-related molecules in IA has not fully understood. Further exploration is warranted to gain a more comprehensive understanding. Neutrophils, the most abundant immune cells in peripheral blood, have garnered increasing attention for their role in disease development [15–17]. Recent research has further revealed that neutrophils in IA patients have been activated peripherally, leading to changes in their RNA expression profile [18]. Nevertheless, the exact role of neutrophils in IA remains incompletely understood, necessitating further investigation.

The release of neutrophil extracellular traps (NETs), a defense mechanism employed by neutrophils [19], comprise a complex network of chromatin DNA, histones, and neutrophil granule proteins [20]. Initially reported in 2004, NETs have demonstrated a crucial influence in bacterial killing by neutrophils [21]. Furthermore, NETs have been implicated in the development and progression of diseases, particularly in those diseases relating to vascular and immune systems [22]. A recent report has suggested a strong association between NETs and atherosclerotic disease, with their components serving as diagnostic biomarkers for this condition [23]. Kato et al. have demonstrated that NETs formation exacerbates sepsis [24]. Similarly, Korai et al. have found that neutrophils promote the rupture of IA through NET formation (NETosis) [25]. A recent animal study has further revealed that inhibiting NETosis has significantly reduced aneurysmal rupture in estrogen-deficient mice compared to controls [26]. Despite accumulating pro-inflammatory evidence for NETs, the precise mechanism of their action in IA remains enigmatic. Therefore, it is imperative to identify convenient and cost-effective biomarkers associated with NETs for IA.

In this study, we aim to investigate the hub genes associated with NETs in IA and construct a risk score model. Using comprehensive bioinformatics tools, our objective is to unravel the functional pathways of these hub genes and comprehensively explore the immune cell infiltration of IAs. Our findings are expected to offer a novel signature for diagnosing and mitigating IA, thereby contributing to enhanced patient outcomes.

Materials and methods

Subjects

The microarray dataset GSE75436 and mRNA expression profile dataset GSE36791 were downloaded from the Gene Expression Omnibus (GEO) database (https://www.ncbi.nlm.nih.gov/geo/). There were 30 samples (15 IAs and 15 controls) in the GSE75436 dataset, which was obtained from the Affymetrix Human Genome U133 Plus 2.0 Array platform. The GSE36791 dataset comprised 18 blood samples from healthy individuals and 43 blood samples from patients with IAs, which was processed on the Illumina HumanHT-12 V4.0 expression bead chip platform.

Weighted gene co-expression network analysis

Weighted gene co-expression network analysis (WGCNA) employs a structured approach to group genes exhibiting similar expression patterns, transforming gene expression into modules. The "WGCNA" package in R software was utilized to build and visualize the network [27]. The network dendrogram was generated for visualization, meanwhile modules were represented by distinct colors, and modules with high similarity were combined. To identify the modules most closely relating to IA, the Pearson correlation analysis was conducted to estimate the relationship among gene modules.

Differentially expressed gene analysis

The differentially expressed genes (DEGs) were screened using "limma" package of R softeare [28] with the cut-off criteria of $|\log_2 FC| > 1$ and p.adjust < 0.05.

Functional enrichment analysis

The Gene Ontology (GO) terms, Kyoto Encyclopedia of Genes and Genomes(KEGG) pathway enrichment analysis and Gene Set Enrichment Analysis (GSEA) were conducted using the "clusterProfiler" R function package [29]. The "DOSE" package of R langue was used to perform disease ontology (DO) analysis. The p-value < 0.05 was considered statistically significant.

Protein–protein interaction (PPI) networks analysis

The STRING database (https://string-db.org/, version 11.0) was employed to delve into the interactions among the proteins encoded by the NETs-related genes, and the Cytoscape (version 3.7.2) was utilized to visualize the resulting protein-protein interaction (PPI) network [30]. The online database GeneMANIA (http://www.genemania.org) was utilized to gain insights into the intricate interactions between proteins and assess potential biological pathways.

Predictive model construction

To further identify the genes associated with NETs, the LASSO Cox regression analysis was performed using the R package "glmnet" (version 4.1-4) [31]. The risk score for each sample was calculated as:

$$\text{Risk score} = \sum_{i=1}^{n} \text{Coef}_i * x_i$$

Where Coef_i was the risk coefficient for each gene, and x_i was the expression of the gene [32]. Patients were subsequently categorized into low-risk and high-risk groups based on the median risk score.

Immune cell infiltration analysis

The "CICERSORT" R package was used to characterize the composition of immune cells for the high-risk group and low-risk group, as well as the IAs group and control group. The proportions of a total of 22 immune cells were calculated for each sample. In addition, four types of immune cell infiltration were estimated using the XCELL database (https://xcell.ucsf.edu/).

Statistical analysis

All statistical analyses were conducted using R software (version 4.2.0). The Wilcox test was applied to assess the difference in continuous variables between the two groups. Statistical significance was considered at $p < 0.05$.

Results

Identification of IA-related modules using WGCNA

To identify potential modules associated with IA, we performed WGCNA on the GSE75436 dataset. The soft power of $\beta = 4$ (Fig. 1A) was determined as soft-thresholding. The results showed that the brown module (r=-0.84, $p < 0.001$) and greenyellow module ($r = 0.87$, $p < 0.001$) were significantly related to IA (Fig. 1B). There was a significant correlation between the module membership and gene significance of the brown and greenyellow modules (Fig. 1C, D). Therefore, these two modules were selected for downstream analysis, containing a total of 2,249 genes (Table S1).

GO and KEGG enrichment analyses of genes in the brown and greenyellow modules were performed to further determine the biological functions of these modules in IA. The results showed that brown module genes were significantly enriched in GO terms such as muscle contraction, contractile fiber, and immune receptor activity (Fig. 1E), interestingly, they were also involved in the biological process of regulation of neutrophil migration (Table S2). The KEGG enrichment results showed that the genes in brown module were significantly involved in 61 pathways such as arginine and proline metabolism and ECM-receptor interaction (Fig. 1F). The greenyellow module genes demonstrated significant enrichment in GO terms such as negative regulation of protein localization, endoplasmic reticulum lumen, and extracellular matrix structural constituent conferring tensile strength (Fig. 1G). Additionally, they were also prominently involved in 16 KEGG pathways like protein digestion and absorption (Fig. 1H). More details of the enrichment were shown in Table S2 and Table S3.

Seven candidate genes related to NETs in IA were screened

To further screen NETs-related candidate genes in IA, we first identified DEGs between IA and control samples. Using the criteria of "$|\log_2 FC| > 1$ and p.adjust < 0.05", a total of 2,823 DEGs were identified in the IA group compared to the control group (Fig. 2A), including 1,534 up-regulated genes and 1,289 down-regulated genes. Moreover, a previously published study has identified 69 genes as initial biomarkers for NETs [33], which were taken as the NETs-related genes. Then, in order to identify NETs-related candidate genes in IA more accurately, the cross-analysis was conducted, which incorporated 2,249 IA-related module genes (basing on WGCNA), 2,823 IA-related DEGs, and 69 NETs-related genes. Next, seven overlapping NETs-related candidate genes were generated and displayed in the Venn diagram (Fig. 2B).

To obtain the potential functional information underlying the seven NETs-related candidate genes, the GO and KEGG enrichment analyses were performed on the above candidate genes. The GO enrichment results showed that the seven candidate genes were enriched in immune-related biological processes, including positive regulation of interleukin-8 production, neutrophil chemotaxis, and regulation of inflammatory response (Fig. 2C, Table S4). Besides, the KEGG pathway enrichment analysis identified immune-related pathways, notably the Toll-like receptor signaling pathway and neutrophil extracellular trap formation (Fig. 2D, Table S4). We thus speculated that these NETs-related candidate genes may play an important role in immune-mediated processes and deserve further attention.

Going further, we performed PPI analysis using the online database STRING, which revealed nine interactions among the seven NETs-related candidate genes (Fig. 2E). We then employed the GeneMANIA network to investigate potential PPI patterns, aiming to deepen our biological understanding of the functional correlations among these seven NETs-related candidate genes. The results identified the top 20 proteins that interact with these candidate genes (Fig. 2F).

Construction and verification of NETs-related diagnostic model in IA

To explore the diagnostic and predictive value of these candidate genes in IA and enhance their clinical

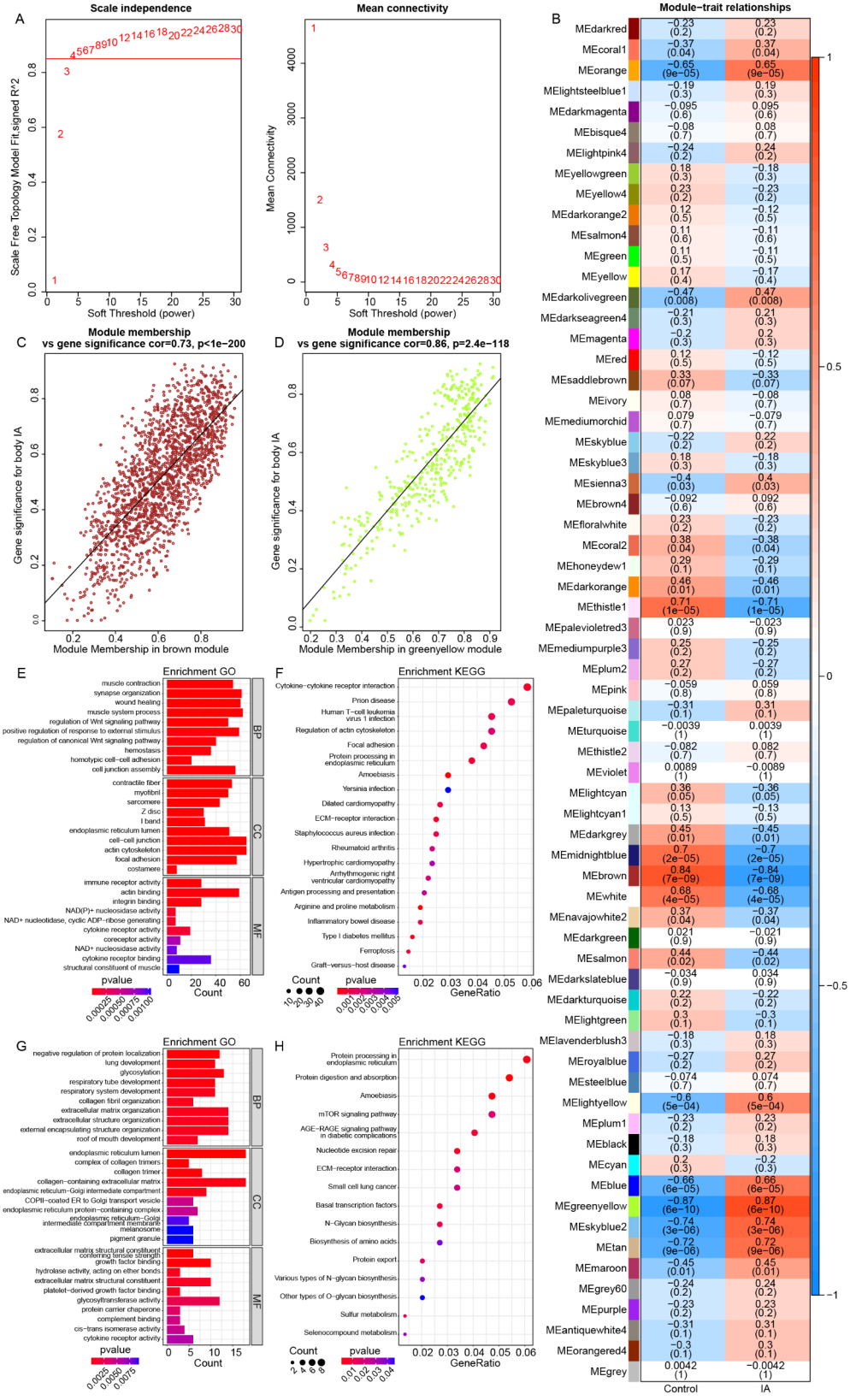

Fig. 1 Co-expression analysis of NETs-related genes in GSE75436 cohort. **(A)**. Determination of the soft-thresholding (power threshold β = 4). **(B)**. Heatmap of the association of gene modules with IA and control groups. Numbers in each cell indicate correlation and significance. **(C, D)**. Scatter plots showing the correlation of genes with the brown module **(C)** and greenyellow module **(D)**. **(E, F)**. The top 10 GO enrichment **(E)** and the top 20 KEGG pathway enrichment **(F)** of brown module genes. **(G, H)**. The top 10 GO enrichment **(G)** and the top 20 KEGG pathway enrichment **(H)** of brown greenyellow genes

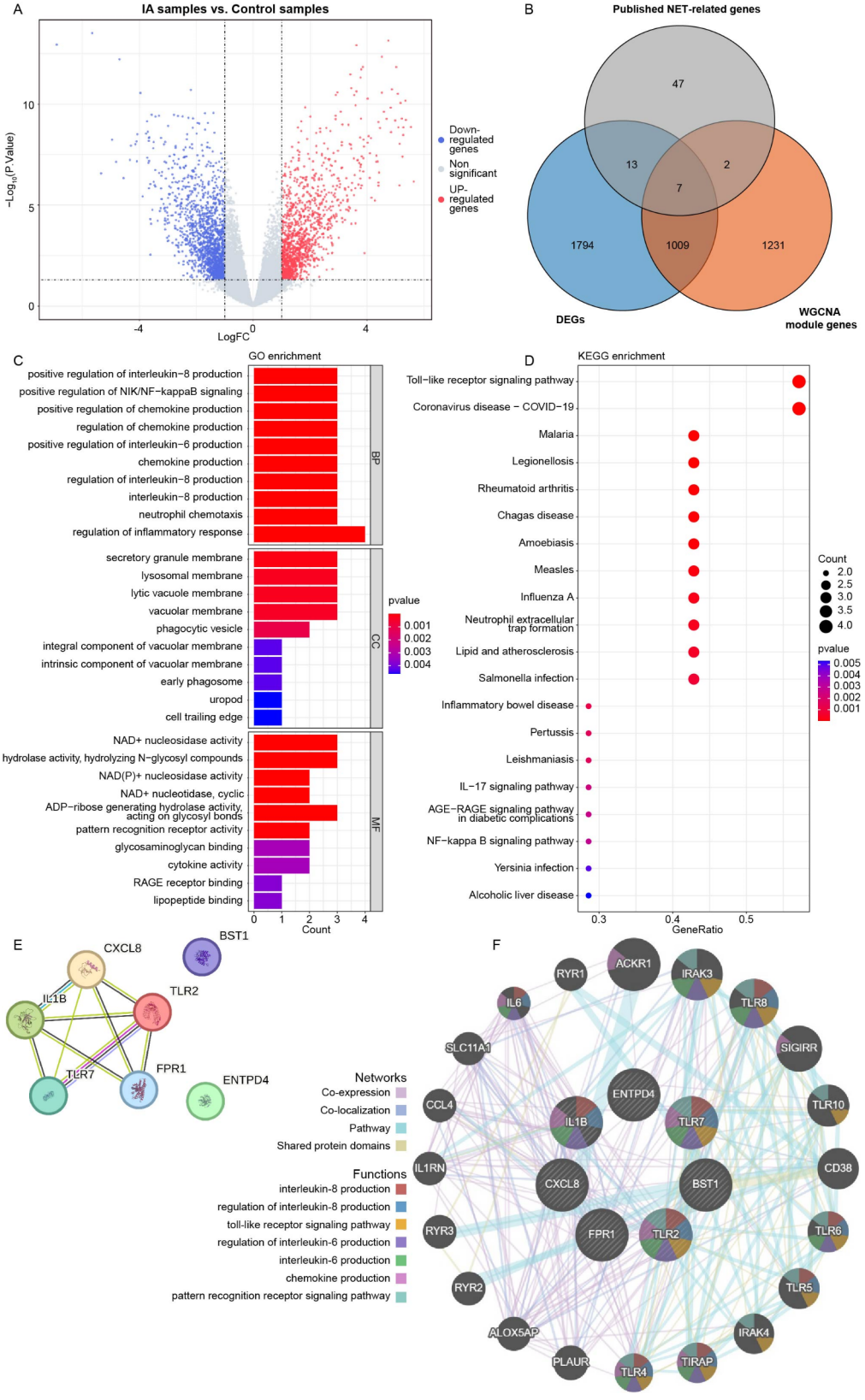

Fig. 2 Identification of candidate genes associated with NETs in IA. (**A**). Volcano plots of DEGs. **(B)**. Venn diagram of the WGCNA module genes, DEGs, and published NETs-related genes. **(C, D)**. The top 10 GO enrichment **(C)** and the top 20 KEGG pathway enrichment **(D)** of candidate genes. **(E)**. PPI network interaction map of candidate genes. **(F)**. Network interaction map of candidate genes based on GENEMANIA

applicability, the machine learning algorithm was used to construct a risk score model. Firstly, we have analyzed the correlation among the seven candidate genes, while no significant strong correlation ($R > 0.8$) among them was found (Fig. S1). We thereby conducted LASSO Cox regression analysis on seven candidate genes, of which five genes (corresponding to the lowest likelihood bias and best imitative effect) were identified as potential optimal genes to build diagnostic model for IA, including *TLR7*, *TLR2*, *IL1B*, *ENTPD4*, and *FPR1* (Fig. 3A, B). Subsequently, a risk score model was constructed, the risk score was calculated based on these five genes' expressions: Risk Score = (*TLR7**0.4189663)+ (*TLR2**0.3784702)+ (*IL1B**0.6492899)+ (*ENTPD4**0.1678660)+ (*FPR1** 0.2000896) (Fig. 3C).

The samples in GSE75436 dataset were stratified into high-risk and low-risk groups using the median risk score value as the cutoff, in order to validate the predictive accuracy of the risk score model. We initially compared the expression levels of the five genes between the high-risk and low-risk groups. Our observations revealed significant differences, the high-risk group exhibiting elevated expression levels compared to the low-risk group (Fig. 3D). Furthermore, we analyzed the expression levels of these genes between IA and control samples in both the GSE75436 and GSE36791 datasets. In the GSE75436 cohort, all five genes were significantly over-expressed in IAs compared to controls (Fig. 3E). In the GSE36791 cohort, all genes except *TLR7* also demonstrated significantly higher expression in the IA group (Fig. 3F). These findings suggested a consistent expression pattern among the majority of these genes in IA, further supporting that they could serve as the NETs-related hub gens for IA. In addition, in both cohorts, IA patients had significantly higher risk scores than the control group (Fig. 3G, H), implying a relatively reliable performance of our risk score. Overall, high risk samples were at a higher predisposition for developing IA.

Exploration of biological significance of NETs-related diagnostic model

To gain deeper insights into the functional role of hub genes related to NETs in IA, we delved into the biological implications of the risk score model. Initially, we conducted DEG analysis comparing high-risk and low-risk groups, and a total of 2,481 DEGs were identified in high-risk group, compared to low-risk group (Fig. 4A). DO enrichment analysis on the 2,481 DEGs showed that they were significantly enriched in 485 DO terms such as demyelinating disease and aortic aneurysm. The top 10 most significant DO terms were shown in Fig. 4B, and all the enrichment results were shown in Table S5.

Then, GSEA enrichment analysis revealed that 128 KEGG pathways were notably enriched under the screening criteria of|NES|>1 and $p < 0.05$ (Table S6). Notably, several pathways, including asthma, intestinal immune network for IgA production, leishmaniasis, systemic lupus erythematosus, and neutrophil extracellular trap formation, among others, were significantly activated in high-risk group (Fig. 4C, S2). On the contrary, cardiac muscle contraction, dilated cardiomyopathy, hypertrophic cardiomyopathy, motor proteins, and regulation of lipolysis in cardiac muscle contraction adipocytes, among other related pathways, were significantly inhibited in patients with IA (Fig. 4D, S2).

In addition, we also conducted GSVA analysis to explore the biological mechanism leading to differences between the high-risk and low-risk groups. We found that some signaling pathways were significantly diversity between the two groups. For instance, the samples in the high-risk group were involved in glycan biosynthesis and toll like receptor signaling pathway (Fig. 4E).

Distinct immune cell infiltration characteristics between different risk score groups

To investigate the association between risk scores and immune status in patients with IA, the CIBERSORT algorithm was utilized to calculate the relative abundance of 22 distinct types of immune cells. We combined the GSE75436 and GSE36791 datasets, called combined-dataset. All IA samples from the combined-dataset were categorized into high-risk-IA and low-risk-IA groups based on the median risk score. The results revealed noteworthy disparities in the proportion of 14 distinct types of immune infiltrating cells between the high-risk-IA and low-risk-IA groups (Fig. 5A). Notably, the high-risk-IA group exhibited a significantly elevated proportion of T cell CD4 + naive, NK cell resting, monocyte, and neutrophil compared to the low-risk-IA group. In contrast, the proportion of lymphocytes, such as B cell plasma and T cell CD4 + memory resting, were significantly lower in the high-risk-IA group. This observation aligns with the recently identified phenomenon of elevated inflammatory cells and reduced lymphocytes in the peripheral blood of patients with IA.

Moreover, the differences in immune cell infiltration between the combined-IA (IA samples in the combined-dataset) and combined-control (control samples in the combined-dataset) groups were also explored. Significant disparities were observed in the infiltration of nine types of immune cells between the combined-control and combined-IA groups (Fig. 5B). Consistent with previous findings, the combined-IA group exhibited a notably higher proportion of monocytes and neutrophils compared to the combined-control group.

Finally, we identified six overlapping immune cell infiltration that exhibited significant differences in both high-risk-IA vs. low-risk-IA and combined-IA

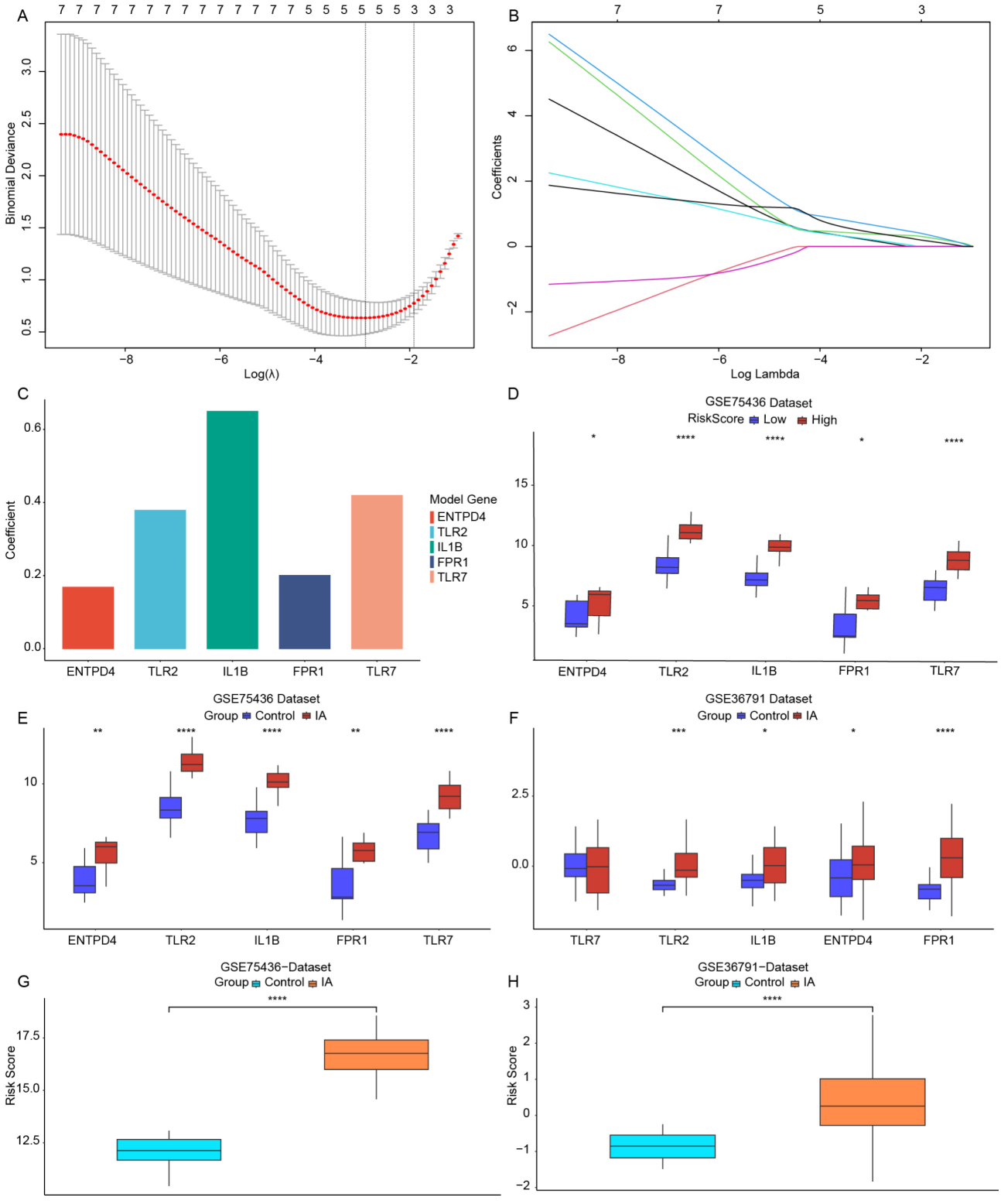

Fig. 3 Construction and verification of risk score model in IA. **(A).** The cross validation curve of the model. X-axis referred to logarithm λ of penalty parameter, and Y-axis represented likelihood bias. The smaller the likelihood bias, the better the imitative effect. **(B)**. The path diagram of regression coefficient. Upper X-axis referred to the number of nonzero coefficient, Y-axis referred to the value of coefficient, and lower X-axis referred to log (λ). Each curve represented the trajectory of the coefficient of independent variable. **(C)**. Coefficient of the five selected hub genes. **(D)**. The expression of hub genes in high-risk and low-risk groups in the GSE75436 dataset. **(E, F)**. The expression of hub genes in IA and control groups in the GSE75436 dataset **(E)** and GSE36791 dataset **(F)**. **(G, H)**. Box plots of the risk score in IA and control groups in the GSE75436 dataset **(G)** and GSE36791 dataset **(H)**

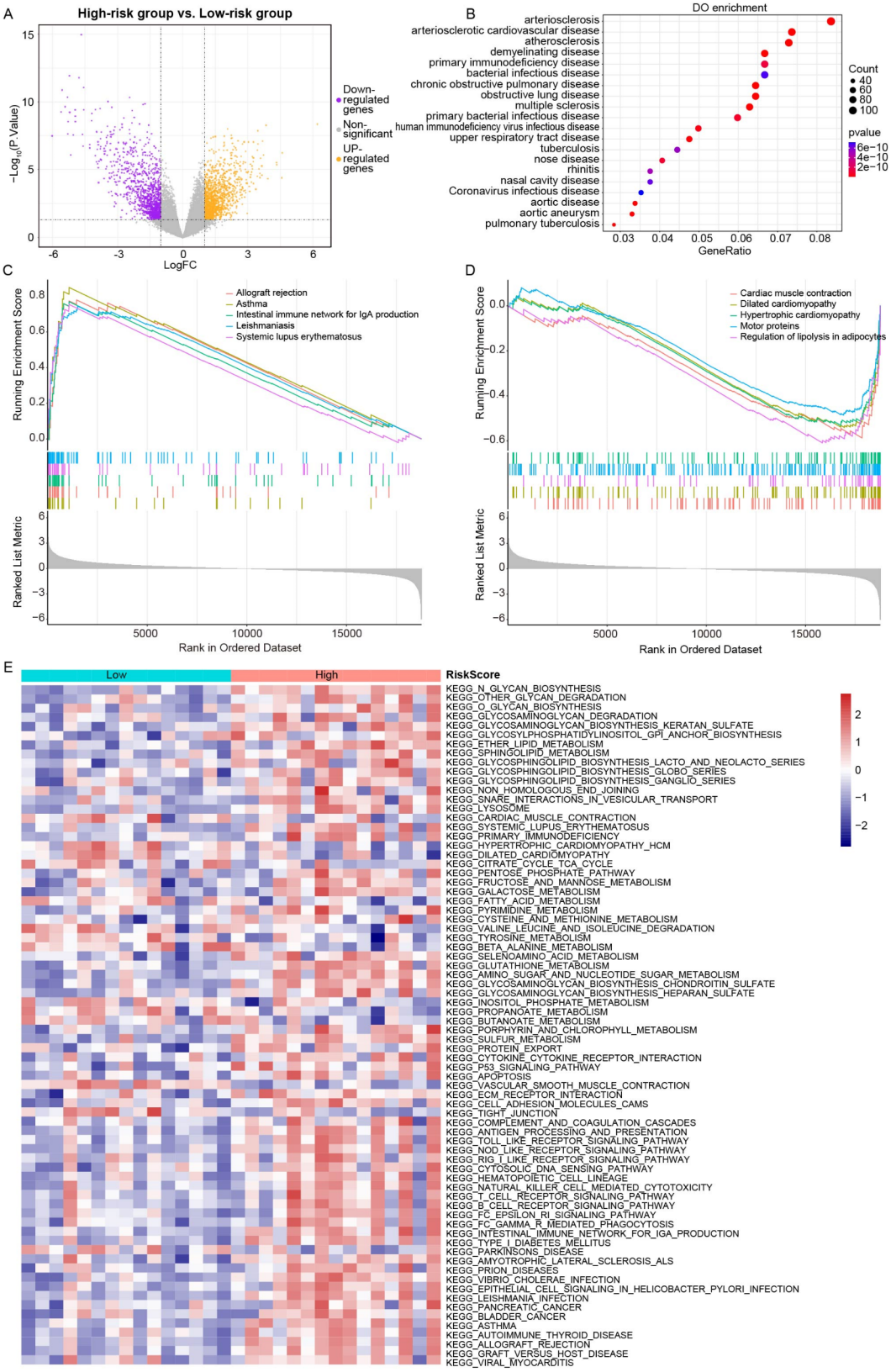

Fig. 4 Exploration of the biological significance of the risk score model. **(A).** Volcano plots of DEGs in high-risk and low-risk groups. **(B)**. The top 20 DO enrichment of DEGs between high-risk and low-risk groups. **(C**, **D)**. The top 5 activated **(C)** and suppressed **(D)** pathways according to $p < 0.05$ based on GSEA. **(E)**. Heatmap of differentially enriched KEGG pathway between high-risk group and low-risk group based on GSVA

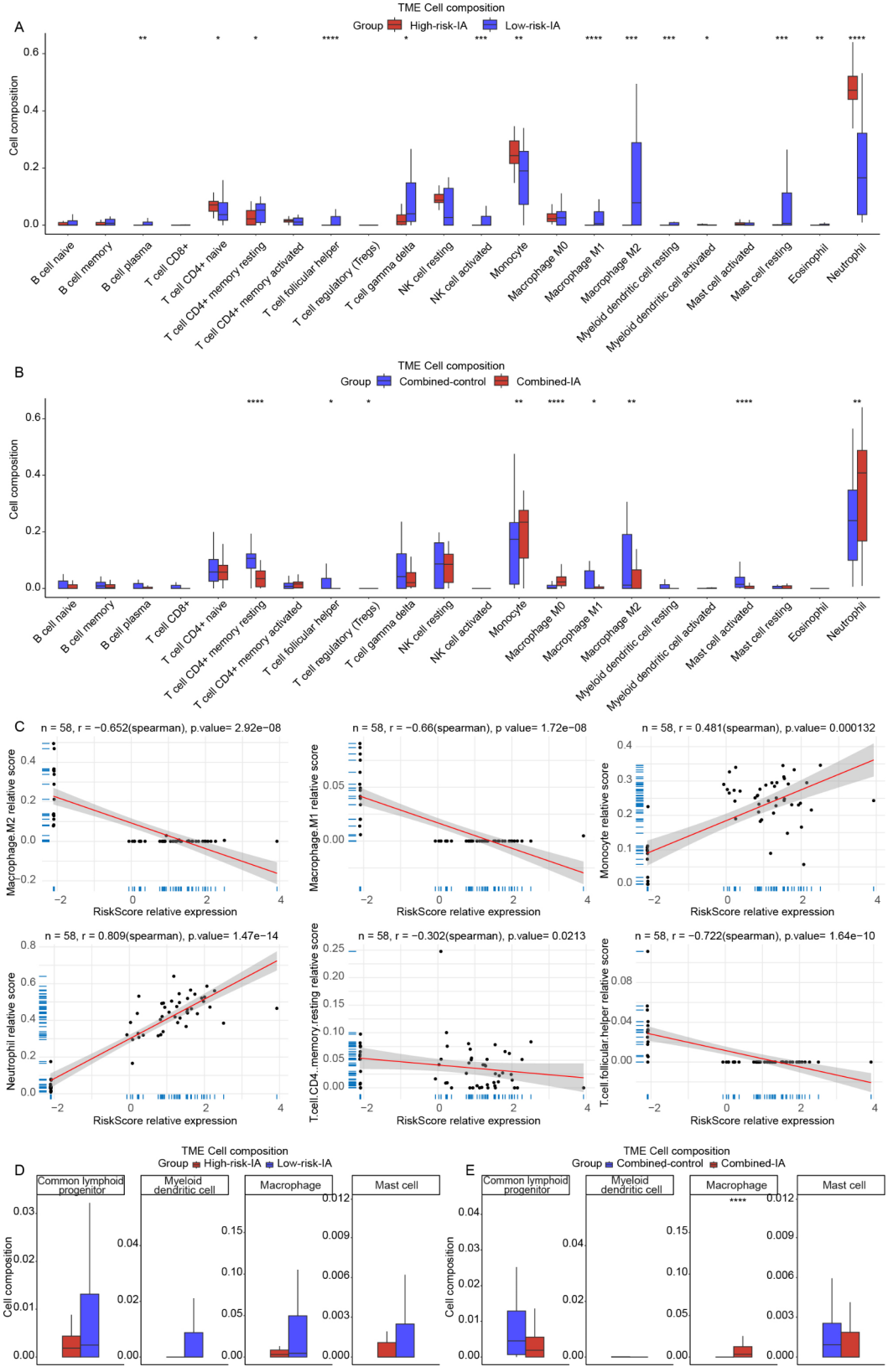

Fig. 5 The landscape of immune cell infiltration in IA patients. **(A).** The immune cell infiltration in the high-risk-IA and low-risk-IA groups. **(B).** The immune cell infiltration in the combined-IA and combined-control groups. **(C)**. Correlation analysis of six immune cells and risk score. **(D**, **E)**. The proportion of four classes of immune cells in the high-risk-IA and low-risk-IA groups **(D)** and the combined-IA and combined-control groups **(E)** based on XCELL

vs. combined-control. In order to further confirm the relationship between the six overlaping immune cell infiltration and risk score, we conducted correlation analysis, revealing a significant positive correlation between monocytes and neutrophils with risk score. Conversely, T cell CD4 + memory resting, T cell follicular helper, macrophage M1, and macrophage M2 exhibited a notable negative correlation with risk score (Fig. 5C).

In addition, we utilized XCELL to analyze the proportions of four distinct immune cell types, including dendritic cells, lymphocytes, macrophages, and mast cells, and found that macrophages had a significant difference in combined-IA compared with the combined-control group. However, no significant differences in other immune cells were observed (Fig. 5D, E).

The risk score model exhibited a good diagnostic performance for IA

To quantitatively evaluate the diagnostic and predictive capabilities of the risk score model, we conducted an ROC analysis using the GSE75436 and GSE36791 datasets. The AUC of the model in the GSE7536 cohort and the GSE36791 cohort were 0.996 and 0.851 (Fig. 6A, B), respectively, indicating that the risk score model exhibited a good diagnostic performance.

Consequently, we proceeded to delve into the drug molecules potentially associated with these five hub genes. Utilizing the DGIdb database, we analyzed the gene-drug interactions and discovered 4, 37, 6, and 12 drugs related to *TLR2*, *IL1B*, *FPR1*, and *TLR7*, respectively (Fig. 6C, Table S7). However, it was unfortunate that no targeted drugs were identified for the prediction of *ENTPD4*.

Discussion

IA is a rare but potentially life-threatening cerebrovascular disease. Before rupture, IA is often asymptomatic, necessitating regular imaging studies for early detection [34, 35]. Immune inflammation plays a pivotal role in the progression and rupture of IA [36]. Biomarkers derived from the transcriptome of circulating neutrophils have shown promise in detecting unruptured IA [18]. NETs were shown to regulate neutrophil development and were involved in inflammation through various mechanisms [37]. However, a limited insight of mechanisms underlying the NETs of IA has hindered progress in diagnostic and therapeutic techniques. Consequently, identifying biomarkers associated with NETs in IA remains an urgent research priority. Here, we have developed a novel diagnostic signature related to NETs in IA.

Initially, we utilized transcriptome data downloaded from GEO to identify seven candidate genes related to NETs in IA. These genes were involved in biological functions such as interleukin-8 production, neutrophil chemotaxis, regulation of inflammatory response, and Toll-like receptor signaling pathway. The Toll-like receptor (TLR), a well-characterized pattern recognition receptor, has been shown to play a crucial role in pathogen recognition and the elicitation of the innate immune response [38]. It was reported that interleukin 8 (IL-8) was a pro-inflammatory cytokine that mainly functioned in the chemotaxis of neutrophils in the blood [39]. Therefore, we postulated that these candidate genes associated with NETs played pivotal roles in immune-mediated processes in IA.

To identify the hub genes related to NETs in IA, we employed LASSO machine-learning techniques to construct a model and identify more precise biomarkers. Ultimately, *TLR7*, *TLR2*, *IL1B*, *ENTPD4*, and *FPR1* were identified as hub genes for IA, and a risk score model was then formulated. Notably, the five hub genes were overexpressed in the high-risk group compared to the low-risk group. We hypothesized that the elevated expression of these five hub genes could serve as a crucial factor in the pathogenesis of IA. To corroborate our findings, we validated the consistency of these expression patterns in an independent dataset. Previously, *TLR2* was found to be significantly up-regulated in IA patients, indicating its crucial role in the development of IA among the Chinese population [40]. More recently, *TLR2* was discovered to be a central gene in atherosclerosis-associated IA, primarily promoting its pathogenesis by activating the inflammatory response and apoptosis mediated by the TLR2-Myd 88-NF-κB pathway [41]. *IL1B* has also emerged as a potential biomarker for IA [42], with its expression level positively correlating with immune cells such as CD8 T cells [43]. Du et al. previously proved that *FPR1* was up-regulated in IA [44], and that its upregulation induces Mac-1-mediated neutrophil synthesis, thereby exacerbating the progression of abdominal aortic aneurysm (AAA) [45]. In summary, our study has reliably identified NETs-related genes. Furthermore, we discovered that IA patients from both cohorts exhibited significantly higher risk scores compared to controls, indicating that individuals with higher risk scores might be more prone to develop IA. These reminded us to intervene in time for patients with high risk scores.

In addition, we conducted a detailed analysis of immune cell infiltration to elucidate the intricate relationship between the risk score model and immune cells. In both the high-risk-IA and combined-IA groups, we observed an abnormal elevation of infiltrating immune cells, including T cell CD4 + naive, NK cell resting, monocyte, and neutrophil, which aligns with previous research findings. NETs played a pivotal role in inflammation and tissue remodeling, leading to an increased risk of aneurysm rupture [25]. Meanwhile, it has been previously documented that under the background of

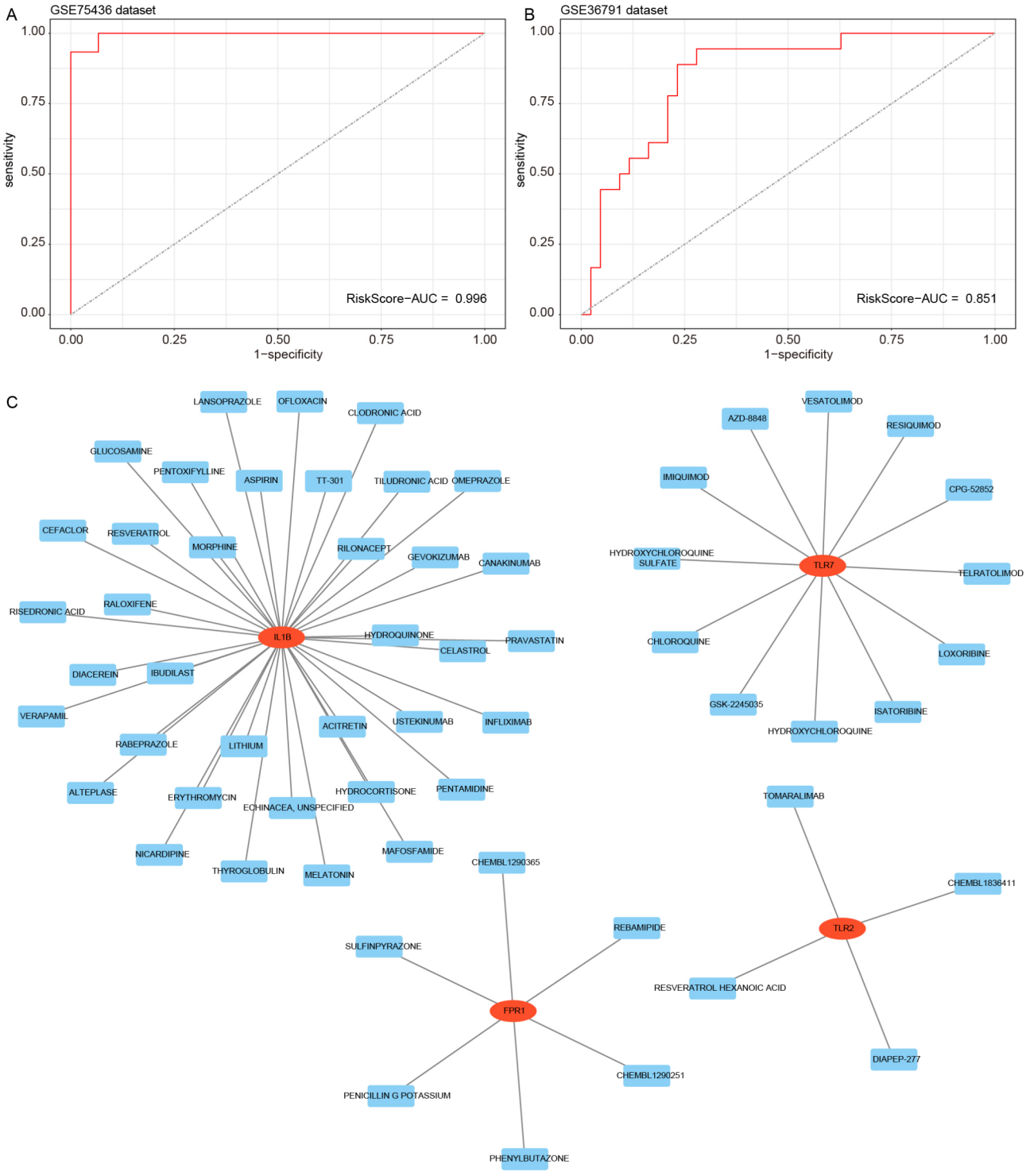

Fig. 6 Clinical value evaluation and drug prediction of risk score module. **(A, B).** ROC curves of the risk score in the GSE75436 dataset **(A)** and GSE36791 dataset **(B)**. **(C)**. Five hub genes target drug network predicted by the DGIdb database

IA, endothelial progenitor cells have exerted crucial role in protecting vascular integrity via replacing injured and dysfunctional endothelial cells [46]. Consequently, in IA, hemodynamic forces trigger endothelial damage and neutrophil activation, leading to the secretion of pro-inflammatory cytokines, neutrophil recruitment, and subsequent NETs formation. Additionally, the enhanced migratory capacity of NK cells in IA patients' peripheral blood promoted their aggregation and activation within the aneurysm wall, thereby contributing to disease

progression [47]. Monocytes were dysregulated in IA patients, favoring a pro-inflammatory response [48]. Correlation analysis further reinforced this finding, revealing a positive association between monocyte and neutrophil infiltration and the risk score. These findings underscored the intimate association between inflammation, immune responses, and IA, highlighting the potential of immune-based therapies in managing this condition.

Conclusions

Our study successfully constructed a risk score model and identified five NETs-related hub genes including *TLR7*, *TLR2*, *IL1B*, *ENTPD4*, and *FPR1* for IA. All five hub genes were significantly up-regulated in both the high-risk group and IA patients and involved in inflammatory response regulation. In conclusion, the risk score model could serve as a promising diagnosis signature for IA. Our study offered novel insights into the pathogenesis and diagnosis of IA, especially involving NETs related roles.

Supplementary Information

The online version contains supplementary material available at https://doi.org/10.1186/s12883-025-04068-w.

Supplementary Material 1: **Figure S1.** The correlation results among seven candidate genes.

Supplementary Material 2: **Figure S2** The top 10 activated and suppressed pathways according to NES1 based on GSEA in the GSE75436 cohort.

Supplementary Material 3

Supplementary Material 4

Supplementary Material 5

Supplementary Material 6

Supplementary Material 7

Supplementary Material 8

Supplementary Material 9

Acknowledgements
Not applicable.

Author contributions
XMZ, HHF, YH conceived and the study, HHF, ZXL, CYH, JCC conducted the experiments, XMZ, JYL analyzed the data, XMZ, HHF wrote the manuscript. All authors read and approved the final version.

Funding
Not applicable.

Data availability
The data that support the findings of this study are available in the Gene Expression Omnibus (GEO) database (https://www.ncbi.nlm.nih.gov/geo/), STRING database (https://string-db.org/, version 11.0), the online database GeneMANIA (http://www.genemania.org), the XCELL database (https://xcell.ucsf.edu/) and the DGIdb database.

Declarations

Ethics approval and consent to participate
Not applicable.

Consent for publication
Not applicable.

Competing interests
The authors declare no competing interests.

Received: 20 October 2024 / Accepted: 4 February 2025
Published online: 19 May 2025

References

1. Etminan N, Rinkel GJ. Unruptured intracranial aneurysms: development, rupture and preventive management. Nat Rev Neurol. 2016;12(12):699–713.
2. Toader C, Eva L, Bratu BG, Covache-Busuioc RA, Costin HP, Dumitrascu DI et al. Intracranial aneurysms and Genetics: an extensive overview of genomic variations, Underlying Molecular Dynamics, inflammatory indicators, and Forward-looking insights. Brain Sci. 2023;13(10).
3. Brown RD. Unruptured intracranial aneurysms. Semin Neurol. 2010;30(5):537–44.
4. Brown RD Jr., Broderick JP. Unruptured intracranial aneurysms: epidemiology, natural history, management options, and familial screening. Lancet Neurol. 2014;13(4):393–404.
5. Macdonald RL, Schweizer TA. Spontaneous subarachnoid haemorrhage. Lancet. 2017;389(10069):655–66.
6. Damiano RJ, Tutino VM, Paliwal N, Patel TR, Waqas M, Levy EI, et al. Aneurysm characteristics, coil packing, and post-coiling hemodynamics affect long-term treatment outcome. J Neurointerv Surg. 2020;12(7):706–13.
7. Tawk RG, Hasan TF, D'Souza CE, Peel JB, Freeman WD. Diagnosis and Treatment of Unruptured Intracranial Aneurysms and Aneurysmal Subarachnoid Hemorrhage. Mayo Clin Proc. 2021;96(7):1970–2000.
8. Jiang H, Ding Y, Wu L, Jiang C, Wang C. The roles and diagnostic value of miRNA-1246 in the serum of patients with intracranial aneurysms. Transl Neurosci. 2022;13(1):172–80.
9. Chen B, Zhou H, Zhou X, Yang L, Xiong Y, Zhang L. Comprehensive Analysis of Endoplasmic Reticulum Stress in intracranial aneurysm. Front Cell Neurosci. 2022;16:865005.
10. Zeyu Z, Yuanjian F, Cameron L, Sheng C. The role of immune inflammation in aneurysmal subarachnoid hemorrhage. Exp Neurol. 2021;336:113535.
11. Kanematsu Y, Kanematsu M, Kurihara C, Tada Y, Tsou TL, van Rooijen N, et al. Critical roles of macrophages in the formation of intracranial aneurysm. Stroke. 2011;42(1):173–8.
12. Wajima D, Hourani S, Dodd W, Patel D, Jones C, Motwani K, et al. Interleukin-6 promotes Murine Estrogen Deficiency-Associated Cerebral Aneurysm rupture. Neurosurgery. 2020;86(4):583–92.
13. Chalouhi N, Points L, Pierce GL, Ballas Z, Jabbour P, Hasan D. Localized increase of chemokines in the lumen of human cerebral aneurysms. Stroke. 2013;44(9):2594–7.
14. Jin J, Duan J, Du L, Xing W, Peng X, Zhao Q. Inflammation and immune cell abnormalities in intracranial aneurysm subarachnoid hemorrhage (SAH): relevant signaling pathways and therapeutic strategies. Front Immunol. 2022;13:1027756.
15. Rosales C, Neutrophil. A cell with many roles in inflammation or several cell types? Front Physiol. 2018;9:113.
16. Frosen J, Piippo A, Paetau A, Kangasniemi M, Niemela M, Hernesniemi J, et al. Remodeling of saccular cerebral artery aneurysm wall is associated with rupture: histological analysis of 24 unruptured and 42 ruptured cases. Stroke. 2004;35(10):2287–93.
17. Tulamo R, Frosen J, Junnikkala S, Paetau A, Pitkaniemi J, Kangasniemi M, et al. Complement activation associates with saccular cerebral artery aneurysm wall degeneration and rupture. Neurosurgery. 2006;59(5):1069–76. discussion 76– 7.
18. Tutino VM, Poppenberg KE, Li L, Shallwani H, Jiang K, Jarvis JN, et al. Biomarkers from circulating neutrophil transcriptomes have potential to detect unruptured intracranial aneurysms. J Transl Med. 2018;16(1):373.
19. Zhang F, Li Y, Wu J, Zhang J, Cao P, Sun Z, et al. The role of extracellular traps in ischemia reperfusion injury. Front Immunol. 2022;13:1022380.

20. Klopf J, Brostjan C, Eilenberg W, Neumayer C. Neutrophil Extracellular traps and their implications in Cardiovascular and Inflammatory Disease. Int J Mol Sci. 2021;22(2).
21. Brinkmann V, Reichard U, Goosmann C, Fauler B, Uhlemann Y, Weiss DS, et al. Neutrophil extracellular traps kill bacteria. Science. 2004;303(5663):1532–5.
22. Hasler P, Giaglis S, Hahn S. Neutrophil extracellular traps in health and disease. Swiss Med Wkly. 2016;146:w14352.
23. Borissoff JI, Joosen IA, Versteylen MO, Brill A, Fuchs TA, Savchenko AS, et al. Elevated levels of circulating DNA and chromatin are independently associated with severe coronary atherosclerosis and a prothrombotic state. Arterioscler Thromb Vasc Biol. 2013;33(8):2032–40.
24. Kato Y, Nishida O, Kuriyama N, Nakamura T, Kawaji T, Onouchi T et al. Effects of Thrombomodulin in reducing lethality and suppressing Neutrophil Extracellular trap formation in the lungs and liver in a Lipopolysaccharide-Induced Murine septic shock model. Int J Mol Sci. 2021;22(9).
25. Korai M, Purcell J, Kamio Y, Mitsui K, Furukawa H, Yokosuka K, et al. Neutrophil Extracellular traps promote the development of intracranial aneurysm rupture. Hypertension. 2021;77(6):2084–93.
26. Patel D, Dodd WS, Lucke-Wold B, Chowdhury MAB, Hosaka K, Hoh BL, Neutrophils. Novel contributors to Estrogen-Dependent Intracranial Aneurysm Rupture Via Neutrophil Extracellular traps. J Am Heart Assoc. 2023;12(21):e029917.
27. Langfelder P, Horvath S. WGCNA: an R package for weighted correlation network analysis. BMC Bioinformatics. 2008;9:559.
28. Ritchie ME, Phipson B, Wu D, Hu Y, Law CW, Shi W, et al. Limma powers differential expression analyses for RNA-sequencing and microarray studies. Nucleic Acids Res. 2015;43(7):e47.
29. Yu G, Wang LG, Han Y, He QY. clusterProfiler: an R package for comparing biological themes among gene clusters. OMICS. 2012;16(5):284–7.
30. Shannon P, Markiel A, Ozier O, Baliga NS, Wang JT, Ramage D, et al. Cytoscape: a software environment for integrated models of biomolecular interaction networks. Genome Res. 2003;13(11):2498–504.
31. Friedman J, Hastie T, Tibshirani R. Regularization paths for generalized Linear models via Coordinate Descent. J Stat Softw. 2010;33(1):1–22.
32. Wang L, Qiu M, Wu L, Li Z, Meng X, He L, et al. Construction and validation of prognostic signature for hepatocellular carcinoma basing on hepatitis B virus related specific genes. Infect Agent Cancer. 2022;17(1):60.
33. Li Q, Chen W, Li Q, Mao J, Chen X. A novel neutrophil extracellular trap signature to predict prognosis and immunotherapy response in head and neck squamous cell carcinoma. Front Immunol. 2022;13:1019967.
34. Wu J, Chen ZJ, Liang J, Lai CS, Li XY, Yang ZJ. Identifying and validating key genes mediating intracranial aneurysm rupture using weighted correlation network analysis and exploration of personalized treatment. Ann Transl Med. 2022;10(19):1057.
35. Roquer J, Cuadrado-Godia E, Guimaraens L, Conesa G, Rodriguez-Campello A, Capellades J, et al. Short- and long-term outcome of patients with aneurysmal subarachnoid hemorrhage. Neurology. 2020;95(13):e1819–29.
36. Gruszka W, Zbroszczyk M, Komenda J, Gruszczynska K, Baron J. The role of inflammation and potential pharmacological therapy in intracranial aneurysms. Neurol Neurochir Pol. 2018;52(6):662–9.
37. Papayannopoulos V. Neutrophil extracellular traps in immunity and disease. Nat Rev Immunol. 2018;18(2):134–47.
38. Duan T, Du Y, Xing C, Wang HY, Wang RF. Toll-like receptor signaling and its role in cell-mediated immunity. Front Immunol. 2022;13:812774.
39. Tsai SJ. Role of interleukin 8 in depression and other psychiatric disorders. Prog Neuropsychopharmacol Biol Psychiatry. 2021;106:110173.
40. Fan J, Yu L, Zhao J. Comparative transcriptome analysis reveals involvement of TLR-2 signaling in the pathogenesis of intracranial aneurysm. J Clin Neurosci. 2018;47:258–63.
41. Zhang Q, Liu H, Zhang M, Liu F, Liu T. Identification of co-expressed central genes and transcription factors in atherosclerosis-related intracranial aneurysm. Front Neurol. 2023;14:1055456.
42. Gao Y, Zhao C, Wang J, Li H, Yang B. The potential biomarkers for the formation and development of intracranial aneurysm. J Clin Neurosci. 2020;81:270–8.
43. Zhou D, Zhu Y, Jiang P, Zhang T, Zhuang J, Li T, et al. Identifying pyroptosis- and inflammation-related genes in intracranial aneurysms based on bioinformatics analysis. Biol Res. 2023;56(1):50.
44. Du G, Geng D, Zhou K, Fan Y, Su R, Zhou Q, et al. Identification of potential key pathways, genes and circulating markers in the development of intracranial aneurysm based on weighted gene co-expression network analysis. Artif Cells Nanomed Biotechnol. 2020;48(1):999–1007.
45. He L, Fu Y, Deng J, Shen Y, Wang Y, Yu F, et al. Deficiency of FAM3D (Family with sequence similarity 3, Member D), a novel chemokine, Attenuates Neutrophil Recruitment and ameliorates abdominal aortic Aneurysm Development. Arterioscler Thromb Vasc Biol. 2018;38(7):1616–31.
46. Ramirez-Velandia F, Mensah E, Salih M, Wadhwa A, Young M, Muram S, et al. Endothelial progenitor cells: a review of Molecular mechanisms in the Pathogenesis and endovascular treatment of intracranial aneurysms. Neuromolecular Med. 2024;26(1):25.
47. Ge P, Liu C, Chan L, Pang Y, Li H, Zhang Q, et al. High-dimensional Immune profiling by Mass Cytometry revealed the circulating Immune Cell Landscape in patients with intracranial aneurysm. Front Immunol. 2022;13:922000.
48. Wang J, Cao Y. Characteristics of circulating monocytes at baseline and after activation in patients with intracranial aneurysm. Hum Immunol. 2020;81(1):41–7.

Publisher's note